DOI 10.1007/s11182-022-02542-3
Russian Physics Journal, Vol. 64, No. 10, February, 2022 (Russian Original No. 10, October, 2021)

MULTISTAGE MARTENSITIC TRANSFORMATIONS IN NANOCRYSTALLINE Ti − 50.9 at.% Ni ALLOY

S. L. Girsova, T. M. Poletika, S. M. Bitter, A. I. Lotkov, and A. N. Kudryashov

UDC 69.018.6: 620.187

Specific features of the spatial distribution of Ti_3Ni_4 *particles in the inhomogeneous grain/subgrain structure of the nanocrystalline* Ti − *50.9 at.%* Ni *alloy are identified depending on the aging temperature. It is found out that the presence of an ensemble of internal interfaces of various types in the nanostructure promotes a heterogeneous distribution of* Ti_3Ni_4 *nanoparticles in the volume of the B2 matrix, which is associated with the precipitation of particles in the region of low-angle subgrain boundaries and the suppression of the decomposition of a solid solution in nanograins with high-angle boundaries. The relationship between the evolution of the system of* Ti_3Ni_4 *precipitates during heat treatment and the staging of martensitic transformations in the nanocrystalline* TiNi *alloy with an inhomogeneous grain/subgrain structure is investigated. It is shown that the difference in the structural-phase states of the substructure and the nanograins is the main reason for the anomalous effect of the R-phase transformation in the sequence of multistage martensitic transformations B2 ↔ R ↔ B19 '.*

Keywords: titanium nickelide, nanocrystalline alloy, annealing, grain/subgrain structure, Ti_3Ni_4 particles, martensite transformations.

INTRODUCTION

Nanocrystalline (NC) TiNi alloys, due to their high strength and functional stability, have been widely used for medical applications [1, 2]. In biomedicine, superelastic TiNi-based alloys with an excessive content of Ni are utilized, which are subjected to aging followed by the formation of coherent Ti_3Ni_4 particles [1−3]. It is well known that precipitation of particles in TiNi polycrystals results in a change of the sequence of martensitic transformations from $B2 \leftrightarrow B19'$ to $B2 \rightarrow R \rightarrow B19'$ [3−5]. The main reason for the multi-stage character of transformations is thought to be the particle distribution heterogeneity in the *B*2-austenite grains, which gives rise to different alloy compositions in terms of Ni in the bulk and at the boundaries [6, 7]. However, the nature of the multistage character in NC TiNi alloys with the dominating volume fraction of internal interfaces remains unclear. There are insufficient research data on the common factors of formation of coherent Ti_3Ni_4 particles and their spatial distribution in the conditions of a nanocrystalline state of the material. The difficulty of studying TiNi-based NC alloys is associated with the necessity to include into consideration such peculiarities as an increase in the critical stresses of the martensitic shear as a result of grain refinement [8], a possibility of suppressing the processes of diffusion-induced disintegration of *B*2-austenite in nanograins [9], a maintenance of high defect density in the nanostructure after severe deformation [10]. Furthermore, an important factor is essential inhomogeneity of TiNi-based alloys after cold deformation treatment. An example is

Institute of Strength Physics and Materials Science of the Siberian Branch of the Russian Academy of Sciences, Tomsk, Russia, e-mail: girs@ispms.tsc.ru; poletm@ispms.tsc.ru; s_bitter911996@mail.ru; lotkov@ispms.tsc.ru; LLC Angioline, Novosibirsk region, industrial settlement Koltsovo, Russia, e-mail: kudryashovan@gmail.com. Translated from Izvestiya Vysshikh Uchebnykh Zavedenii, Fizika, No. 10, pp. 124–130, October, 2021. Original article submitted February 15, 2021.

TABLE 1. Martensitic Transformation Temperatures in Ti – 50.9 at.% Ni Alloy Specimens

T annealing	T_R, °C	M_s, °C	M_f, °C	A_s, °C	A_f,°C
Initial	7	−74	−140	−45	−26
300°C	22	−50	−130	−37	−14
400°C	33	−30	−115	−2	15

a mixed grain-subgrain $B2$-austenite structure, which is typical for the NC TiNi textured specimens after severe cold deformation [11]. A similar structure is exhibited by the products designed for manufacturing the miniature medical application systems (wires, thin-wall tubes, etc).

The purpose of this work is to study the effect of the grain-subgrain nanostructure on the size and spatial distribution of Ti_3Ni_4 particles in a NC Ti − 50.9 at.% Ni alloy during aging and on the multistage martensitic transformations.

MATERIALS AND METHODS

The experimental material was a commercial nanocrystalline Ti − 50.9 at.% Ni alloy (Vascotube GmbH, Germany). The specimens were cut from the microtubes designed for manufacturing medical stents. The specimens were annealed with holding for 1 h at 300°C (low-temperature aging) and at 400°C (temperature interval of intensive precipitation of Ti_3Ni_4 particles). These temperatures allow generating Ti_3Ni_4 particles of various sizes and differing morphology. The heat treatment was performed in a salt bath with an automatic temperature control. After holding for the given time the specimens were quenched into water at room temperature.

The start and finish temperatures of the forward and reverse $B2 \leftrightarrow R \leftrightarrow B19'$ martensitic transformations were determined by measuring the electrical resistivity. In order to study the multistaging transformation features, the specimens were additionally examined by the DSC method in a NETZSCH DSC 404 F1 differential scanning calorimeter at a heating/cooling rate of 10 K/min. The structural TEM studies of the specimens cut along the tube axis were carried out in a JEM 2100 (JEOL) transmission electron microscope. The thin foil preparation procedure involed grinding and mechanical polishing of the specimen to a thickness of 1 mm, followed by ion thinning in an EM 09100IS (JEOL) device. The average grain and subgrain sizes were determined by measuring the average diameters of as many as 100 grains in the bright- and dark-field images. A comparative analysis of the Ti_3Ni_4 precipitates was performed versus the treatment conditions using (primarily) the dark-field images. The critical temperatures of the start of the $B2 \rightarrow R$ (T_R) martensitic transformations and the start (M_s, A_s) and finish (M_f, A_f) of the forward (M_s, M_f) and reverse (A_s, A_f) $R \rightarrow B19'$ martensitic transformations, which were determined by measuring the electrical resistivity, are given in Table 1. The $B2 \leftrightarrow R \leftrightarrow B19'$ sequence of forward and reverse martensitic transformations is observed for all experimental alloy specimens.

RESULTS AND DISCUSSION

Grain-subgrain nanostructure

The initial Ti−50.9 at.% Ni alloy has an inhomogeneous hierarchically organized grain-subgrain $B2$-austenite nanostructure containng the elements of two scales: (i) conglomerates of slightly misoriented nanosubgrains of micron dimensions and (ii) nanograins with high-angle boundaries included into the substructure regions, which provides a large variety of internal boundaries (Fig. 1).

There are two types of nanograins: (i) strain-induced nanograins, which are formed during severe deformation followed by annealing, generally contain residual dislocations; (ii) dislocation-free nanograins crystallized from the amorphous state [11]. The dislocation-free nanograins with high-angle boundaries have the average size of 70 nm. The subgrains measuring 40−60 nm contain high-density dislocations, have imperfect small-angle boundaries with an

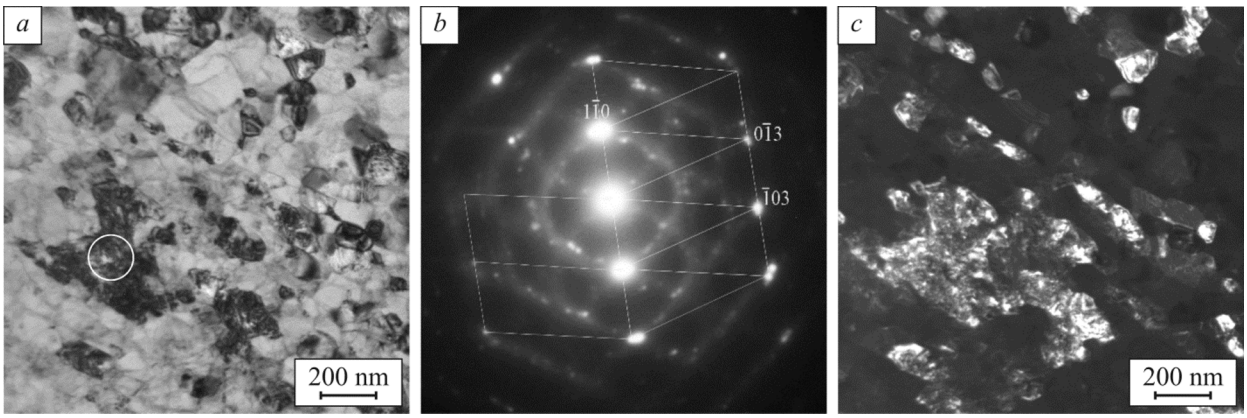

Fig. 1. Mixed grain-subgrain structure: *a* – bright-field image, *b* – corresponding microdiffraction, *c* – dark-field image in the {1T0} (221) reflection of the *B*2-austenite from the region indicated by a circle in (*a*) there are groups of subgrains forming a region of submicron dimensions.

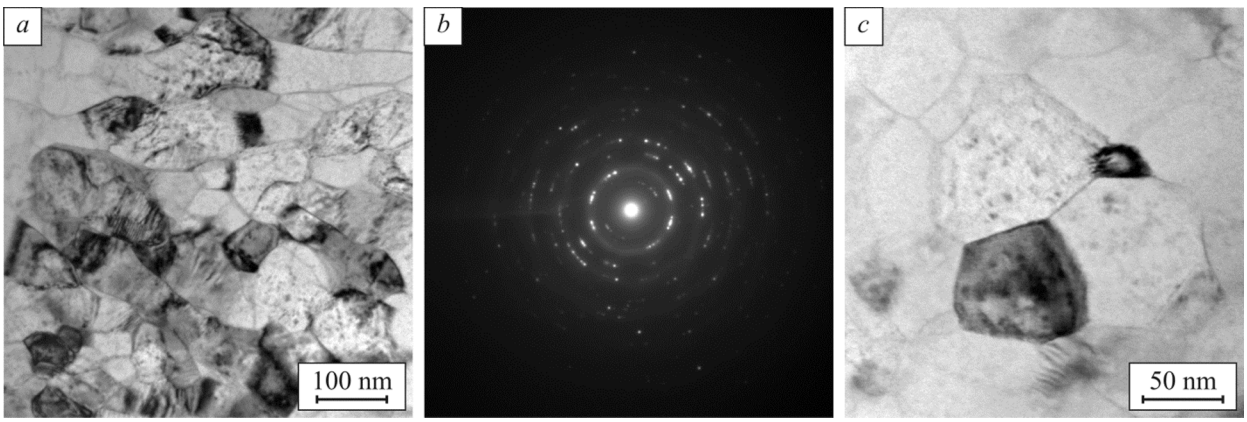

Fig. 2. Structure after annealing at 300°C: *a* – bright-field image, *b* – corresponding microdiffraction pattern, aperture diameter –1.2 μm, there are no reflections from the Ti_3Ni_4 precipitates due their minor size, *c* – bright-field image revealing the presence of fine coherent Ti_3Ni_4 precipitates with a typical diffraction contrast referred to as 'coffee bone'.

azimuthal misorientation of smaller than 3°, and form the regions of micron dimensions (about 800 nm) (Fig. 1*b*). The microdiffraction patterns, corresponding to the grain-subgrain structure, mainly have the character of ring-shaped point reflections. In addition to the reflections from the *B*2-austenite, there are individual reflections that could be attributed both to the *R*-phase and Ti_3Ni_4 particles.

Low-temperature aging

Annealing at 300°C is accompanied by the processes of recovery and polygonization, dislocation density decrease, and straitening of low-angle boundaries, but does not give rise to any appreciable change of the grain/subgrain sizes. Figure 2*a*, *c* presents the bright-field images of the alloy structure, which demonstrate precipitation of coherent globular Ti_3Ni_4 nanoparticles with the sizes smaller than 5 nm, which is typical for the initial stage of disintegration of the TiNi *B*2-solid solution in the course of low-temperature aging [12]. The Ti_3Ni_4 particles are mainly located inside subgrains on dislocations. The presence of highly-dispersed coherent Ti_3Ni_4 phases is indicated by the appearance of

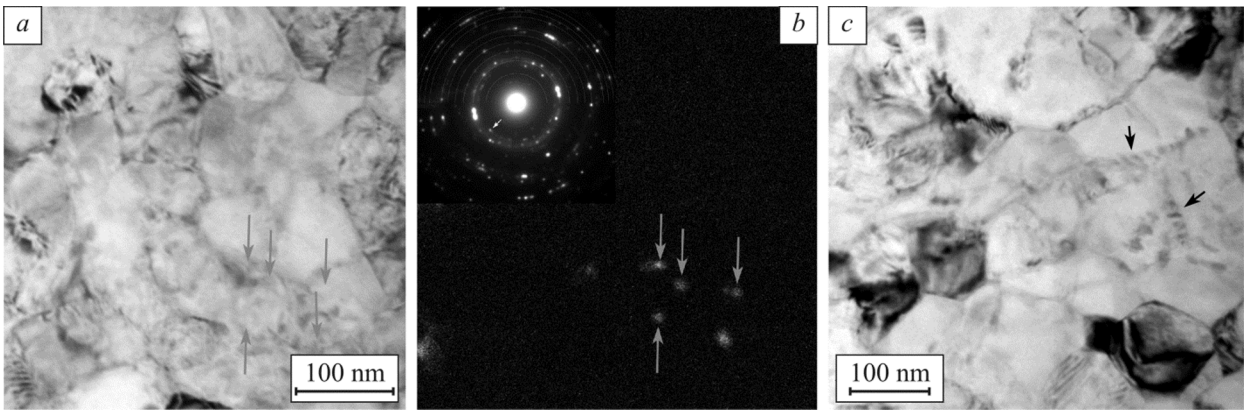

Fig. 3. Subgrain structure with Ti_3Ni_4 particles after annealing at 400°C: *a*, *c* bright-field images; arrows in (*a*, *c*) indicate the rows at the low-angle sub-boundaries; arrows in (*b*) indicate the particles visible in the dark field in the {012} reflection of Ti_3Ni_4 in the microdiffraction pattern (*b*).

weak reflections in the 1/7 positions along the *B*2-lattice in the <321> orientation. A group of subgrains is observed in Fig. 2*c,* which contain coherent Ti_3Ni_4 particles with a characteristic diffraction contrast in their vicinity due to the elastic distortion fields.

It should be noted that Ti_3Ni_4 precipitates are available in the nanograins containing dislocations, but there are none in the dislocation-free nanograins. Moreover, Ti_3Ni_4 nanoparticles are seldom observed in the region of boundaries/sub-boundaries, which is due to the low aging temperature (300°C) not favoring the diffusion of Ni atoms from the inner part of the grains/subgrains into their boundaries [13]. Our results are consistent with the data [13] for polycrystalline TiNi alloys indicating that a low-temperature annealing (at $T < 330$°C) leads to precipitation of a large number of coherent spherical nanoparticles with a diameter of <10 nm [13].

As it was noted above, nanograins in the grain-subgrain structure can be of different nature: nanograins of deformation origin crystallized from the amorphous state, which contain dislocations, and dislocation-free nanograins crystallized from the amorphous state [11]. Unfortunately, it is impossible to reliably determine the type of nanograins observed in every case without a special examination. One can however suppose that the absence of Ti_3Ni_4 nanoparticles in the dislocation-free nanograins can indicate that a necessary condition for particle precipitation during low-temperature aging is the availability of dislocations. This is consistent with the data reported by Hu et al. [14], who demonstrate that TiNi nanograins, crystallized form the amorphous state, do not primarily meet the energy requirements for the Ti_3Ni_4 to precipitate due to the energy released as a result of crystallization. It is worthy of note that a suppression of the diffusion-induced disintegration of the *B*2-solid solution of TiNi in the dislocation-free nanograins and the formation of coherent Ti_3Ni_4 particles agrees with the data on the absence of *R*-phase in them, which primarily nucleates from the particle–matrix interfaces [2, 6, 15].

High-intensity aging at 400°C

During annealing at 400°C the dislocation density in the subgrian structure is observed to decrease and the scatter of the size distribution of polygonized nanograins is observed to increase, which indicates the absence of recrystallization. Redistribution of the dislocations inside the subgrains during the recovery is followed by their annihilation or departure to low-angle sub-boundaries, which results in a change of the structure and shape of the latter: (i) the shape of sub-boundaries changes from that straightened after annealing at 300°C (Fig. 2) to a convex shape at 400°C (Fig. 3); (ii) there appears a blurred diffraction contrast in the bright-field images of sub-boundaries (Fig. 3), which can indicate their non-equilibrium state [16, 17]. The latter circumstance is due to a considerable distortion of the *B*2-matrix in the fields of elastic stresses generated by the excessive dislocations and Ti_3Ni_4 formed in the region of sub-boundaries [17].

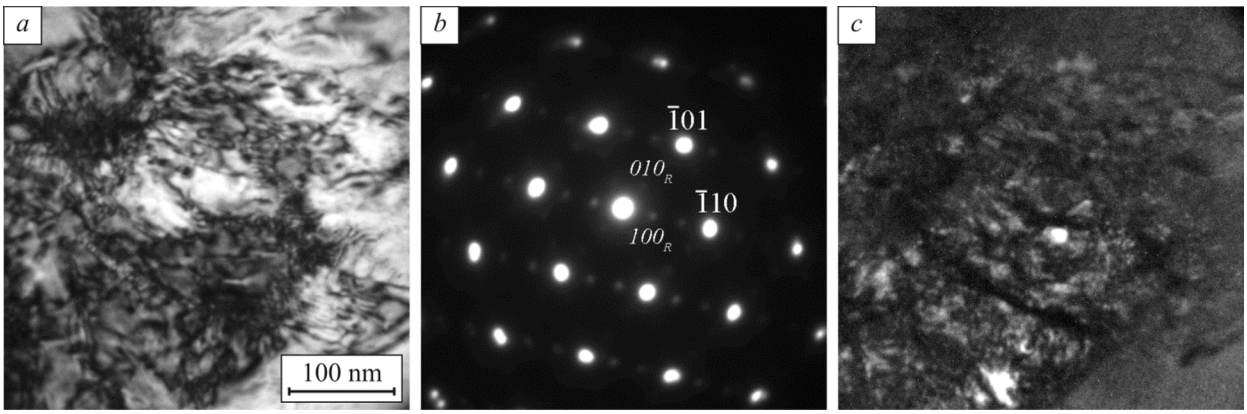

Fig. 4. *R*-phase in the substructure: *a* – bright-field image of a complex deformation contrast simultaneously generated by Ti_3Ni_4 particles, dislocations and *R*-phase, *b* – microdiffraction pattern from (*a*); *c* – respective dark-field image in the {010} reflection of *R*-phase; the disperse *R*-phase is visible.

During annealing at 400°C, aging is quite intensive, which is due to the highest rate of precipitation of Ti_3Ni_4 particles in the temperature interval of 400−450°C [18]. The micro diffraction patterns contain numerous point ring-shaped reflections (Fig. 3) belonging to *R*-martensite and Ti_3Ni_4-phase precipitates. It is evident in Fig. 3 that Ti_3Ni_4 particles precipitate mainly in the region of nonequilibrium sub-boundaries. It is noteworthy that the particles acquire a nearly lens-like shape, a transverse size of up to 5 nm, and a length of up to 20 nm. There is a tendency for the particles to arrange into rows in the planes of the {111} type. The rows of Ti_3Ni_4 particles adjacent to the sub-boundaries are clearly seen in Fig. 3*a*, *c*, which indicates an autocatalytic nucleation character necessary for the compensation of their nucleation and growth energy [5].

The peculiarities of the Ti_3Ni_4 particle morphology in the substructure should be added with the fact that the particles lose their lens-like shape caused by the mismatch between the crystal lattices of the particles and the *B*2-matrix [5]. One might take that this is due to the asymmetric particle growth in the presence of high local inhomogeneous stress fields near the sub-boundary [5, 19]. No lens-shaped Ti_3Ni_4 particles and their rows in nanograins with high-angle boundaries have been observed. This is consistent with the conclusions made by Prokofiev et al. [9] on a possible suppression of the disintegration of the *B*2-solid solution followed by the formation of Ti_3Ni_4 particles in the grains smaller than 150 nm in size in the TiNi alloy aged at 400°C. The main reason is thought to be the complexity of formation of self-accommodated particle arrays inside the NC grains due to geometrical constraints [5, 6]. Therefore, the type of internal boundaries of the subgrains/grains and the long-range stress fields generated by these boundaries are the principal factors affecting the process of heterogeneous nucleation of coherent Ti_3Ni_4 particles in the nanocrystalline TiNi alloy having a grain-subgrain structure in the temperature interval of an intensive diffusion-induced disintegration of the *B*2-austenite. The particle nucleation at the low-angle boundaries and the suppression of disintegration of the *B*2-solid solution are mainly observed in the nanograins with high-angle boundaries.

After annealing at 400°C, the alloy at room temperature is found in a two-phase state, *B*2 + *R* (Table 1). Given a constant grain/subgrain size, we might take that an intensive precipitation of Ti_3Ni_4 particles would effectively reduce the concentration of Ni in the *B*2 matrix and increase the *B*2↔*R* transformation temperature (T_R). The *R*-martensite is dispersed and consists of nanodomains measuring smaller than 10 nm, its morphology is mostly imperfect (Fig.4*c*), which is due to the influence of the elastic stress fields generated by coherent Ti_3Ni_4 particles and dislocations. There is *R*-martensite in the substructure, but there is none in the nanograins which do not contain any dislocations or particles. An *R*-martensitic transformation can completely involve the individual grains and their groups (Fig. 4).

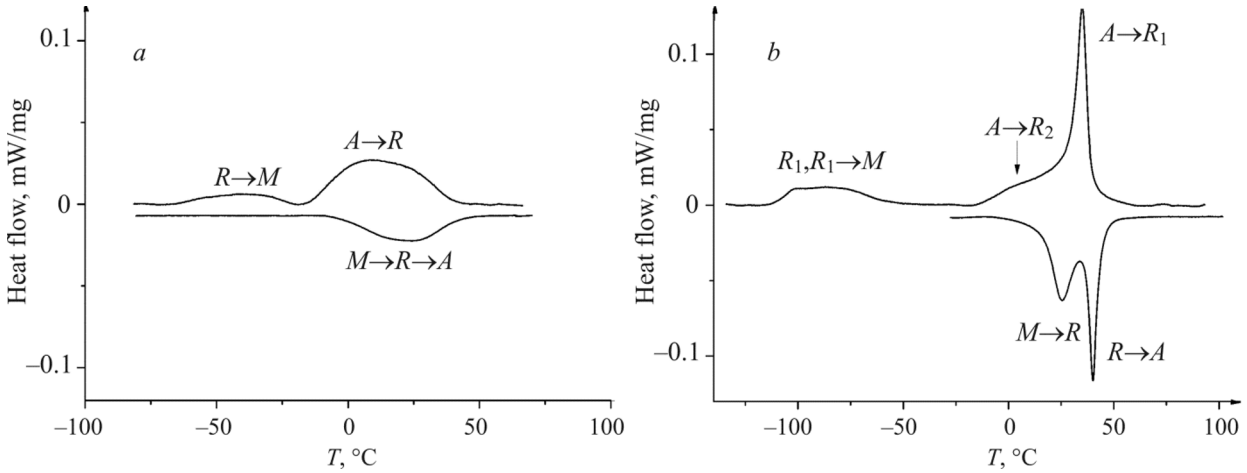

Fig. 5. DSC curves of cooling (top) and heating (bottom) of the Ti – 50.7% Ni alloy after its isothermal annealing at 300°C (*a*) and 400°C (*b*) for 1 hour.

Multistage martensitic transformations

In polycrystalline TiNi alloys, two types of structural inhomogeneity are commonly studied, which could distort the sequence of martensitic transformations: (i) local inhomogeneity of the Ni atom concentration and internal stresses near the coherent Ti_3Ni_4 particles; (ii) microinhomogeneity due to the differing character of the disintegration of the *B*2-solid solution of TiNi between the grain-boundary region and the bulk of the grains [4−7]. The version proposed by Ravari et al. [20] is thought to be most suitable: they think that the reason for the multistage character of martensitic transformation is the presence of certain zones in the alloy, where the particle sizes or their distribution densities are different. For instance, the inhomogeneity of Ti_3Ni_4 particle distribution inside the grains gives rise to the different Ni concentrations in the *B*2-austenite in the boundaries and in the bulk of the grains. As a result, the $B2 \leftrightarrow R$ transformation first occurs at the grain boundary with a low concentration of Ni atoms and then inside the grains with a larger Ni content.

It is evident that the grain size determines the ratio of the volume fraction of the grain-boundary region to the inner part of the grains and can influence the distribution of Ti_3Ni_4 particles and martensitic transformations of the aged polycrystalline specimens [7, 21]. It is noteworthy that according to [22], the zones depleted in Ni in the vicinity of the particle–matrix interface vary from 20 to 100 nm depending on the precipitate size, which is consistent with the observed size range of the structural elements of the NC TiNi alloy structure and makes it possible to focus only on the local composition inhomogeneity in terms of Ni. At the same time, the results obtained in this study allow identifying the structure inhomogeneity related to the differing character of Ti_3Ni_4 precipitation in the substructure and in individual nanograins. In particular, after aging at 400°C, there appears an inhomogeneity of the concentration of Ni atoms in the *B*2-matrix due to their different concentrations in the substructure regions and groups of nanograins. This concentration inhomogeneity is characterized by the submicron scale and is higher than the local inhomogeneity of stresses and the Ni concentration near the Ti_3Ni_4 particles. In this case, an anomalous effect of a two-stage *R*-transformation is possible, during which an *R*-phase with a higher $B2 \leftrightarrow R_1$ transformation temperature is formed in the substructure region, where there are Ti_3Ni_4 precipitates, while the nanograins free from the precipitates are characterized by a lower $B2 \leftrightarrow R_2$ transformation temperature.

A study of the martensitic transformations by the method of differential scanning calorimetry (DSC) has proved our suppositions. For comparison, Fig. 5 presents the DSC curves for the specimens annealed at 300 and 400°C. After aging at 300°C, there are two smeared exothermic peaks (Fig. 5*a*), which are due to the forward $B2 \rightarrow R$ and $R \rightarrow B19'$ transformations. This is typical for the TiNi alloys with the defective *B*2 austenitic structure in an aged state [20] and

indicates a normal single-stage $B2 \rightarrow R$ transformation. During heating, there is a single broad endothermic peak corresponding to the $B19' \rightarrow R \rightarrow B2$ transformations. After annealing at 400°C under the conditions of intensification of aging, the DSC curves of the alloy demonstrate a different behavior (Fig. 5*b*). There are two peaks during cooling, which correspond to the $B2 \rightarrow R_1$ and $B2 \rightarrow R_2$ transformations in the substructure and in the nanograins, respectively. The bases of peaks merge, which makes their separation with a sufficient accuracy impossible. An intensive precipitation of the Ti_3Ni_4 particles causes a shift of the $B2 \rightarrow R$ transformation towards higher temperatures; the *R*-phase is stabilized, which inhibits the $R \rightarrow B19'$ transformation displacing it towards the region of low temperatures. Smearing of the exothermic peak, corresponding to the $R \rightarrow B19'$ transformation, is due to the inhomogeneous spatial distribution of the particles and corresponds to the R_1, $R_2 \rightarrow B19'$ transformation extended in terms of the temperature. During heating, two merging, but quite narrow and clearly distinguishable, peaks are recorded, which correspond to the consecutive $B19' \rightarrow R$ and $R \rightarrow B2$ transformations (Fig. 5*b*).

CONCLUSIONS

An electron microscopy study of the sizes and morphology of the coherent Ti_3Ni_4 particles precipitated at the aging temperatures of 300 and 400°C in the nanocrystalline Ti − 50.9 at.% Ni alloy with an inhomogeneous hierarchically organized grain-subgrain *B*2 austenitic nanostructure has been performed.

It has been shown that during low-temperature aging at 300°C there is precipitation of coherent spherical Ti_3Ni_4 nanoparticles less than 5 nm in size on the dislocations mainly in the substructure. The Ti_3Ni_4 particles are observed in the nanograins containing dislocations but none of them are found in the dislocation-free nanograins.

It has been found out that along with the increase in the size of the Ti_3Ni_4 nanoparticles and the change of their shape from the spherical to a nearly lens-like shape, there is a change of their spatial distribution from location on the dislocations to precipitation on the sub-boundaries. The presence of an ensemble of varying-type internal boundaries in the TiNi nanostructure is the major factor influencing the process of heterogeneous nucleation of the coherent Ti_3Ni_4 particles in the temperature interval of their intensive precipitation (400°C). The particles nucleate at low-angle sub-boundaries and the decomposition of the *B*2 solid solution is suppressed mainly in the nanograins with large-angle boundaries.

The inhomogeneous distribution of the Ti3Ni4 particles in the grain-subgrain nanostructure of the TiNi alloy provides a different structural-phase state of the structure elements (subgrains, nanograins), which results in different Ni concentrations in the *B*2 austenite in the subgrain and nanograins regions and is one of the reasons for the anomalous effect of the two-stage *R*-transformation $B2 \leftrightarrow R_1$, R_2 in the $B2 \leftrightarrow R \leftrightarrow B19'$ sequence.

The results obtained in this study will be used in selecting the heat treatment regimes in the production process of manufacturing Russian blood vessel stents from a TiNi-based alloy, which would provide high technical and functional material characteristics.

This work was carried out within the Government Research Assignment for ISPMS SB RAS, Project No. FWRW-2021-0004.

REFERENCES

1. M. H. Elahinia, M. Hashemi, M. Tabesh, and S. B. Bhaduri, Prog. Mater. Sci., **57**, 911 (2012).
2. K. Otsuka and X. Ren, Prog. Mater. Sci., **50**, 511 (2005).
3. Y. Zheng, F. Jiang, L. Li, H. Yang, and Y. Liu, Acta Mater., **58**, 3444 (2010).
4. G. L. Fan, W. Chen, S. Yang, *et al*., Acta Mater., **52**, 4351 (2004).
5. J. Khalil-Allafi, A. Dlouhý, and G. Eggeler, Acta Mater., **50**, 4255 (2002).
6. J. Khalil-Allafi, X. Ren, and G. Eggeler, Acta Mater., **50**, 793 (2002).
7. X. Wang, S. Kustov, K. Li, *et al*., Acta Mater., **82**, 224 (2015).
8. X. Shi, L. Cui, D. Jiang, *et al*., Smart Mater. Struct., **24**, 072001 (2015).
9. E. A. Prokofiev, A. Burow, E. Payton, and S. Bhaduri, Memory Alloys. Adv. Eng. Mater., **12**, 747 (2010).

10. S. Prokoshkin, V. Brailovski, S. Dubinskiy, *et al*., Shap. Mem. Superelasticity, **2**, 12 (2016).
11. S. Prokoshkin, S. Dubinskiy, and V. Brailovski, Shap. Mem. Superelasticity, **5**, 336 (2019).
12. M. Nishida, C. M. Wayman, and T. Honma, Metall. Trans., **A17**, 1505 (1986).
13. J. I. Kim, S. Miyazaki, Acta Mater., **53**, 4545 (2005).
14. L. Hu, S. Jiang, and Y. Zhang, Metals, **7**, 145 (2017).
15. A. Dlouhy, J. Khalil-Allafi, and G. Eggeler, Phil. Mag., **83**, 339 (2003).
16. R. Z. Valiev, R. K. Islamgaliev, I. V. Alexandrov, Prog. Mater. Sci., **45**, 911 (2000).
17. X. Sauvage, G. Wilde, S. V. Divinski, *et al*., Mater. Sci. Eng. A, **540**, 1 (2012).
18. A. R. Pelton, S. M. Russell, and J. DiCello, JOM, **55**, 33 (2003).
19. S. Cao, C. B. Ke, X. P. Zhang, and D. Schryvers, J. Alloys Compd., **577**, 215 (2013).
20. B. K. Ravari, S. Farjami, M. Nishida, Acta Mater., **69**, 17 (2014).
21. X. Wang, B. Verlinden, and J. Van Humbeeck, Intermetallics, **62**, 43 (2015).
22. Z. Yang, W. Tirry, and D. Schryvers, Scr. Mater., **52**, 1129 (2005).